The Helix-to-Sheet Transition of an HIV-1 Fusion Peptide Derivative Changes the Mechanical Properties of Lipid Bilayer Membranes

William T. Heller[1,*] and Piotr A. Zolnierczuk[2]

[†]Neutron Scattering Division, Oak Ridge National Laboratory, Oak Ridge, TN, 37831, [‡] Forschungszentrum Jülich GmbH, Jülich Centre for Neutron Science at SNS, Oak Ridge National Laboratory, Oak Ridge, TN 37831.

***Corresponding Author**

Email hellerwt@ornl.gov; Phone: 865-241-0093

Note

The authors declare no competing financial interests

Notice: This manuscript has been authored by UT-Battelle, LLC, under contract DE-AC05-00OR22725 with the US Department of Energy (DOE). The US government retains and the publisher, by accepting the article for publication, acknowledges that the US government retains a nonexclusive, paid-up, irrevocable, worldwide license to publish or reproduce the published form of this manuscript, or allow others to do so, for US government purposes. DOE will provide public

access to these results of federally sponsored research in accordance with the DOE Public Access Plan (http://energy.gov/downloads/doe-public-access-plan).

Abstract

A short sequence on the gp41 envelope protein of HIV-1 is integral to infection by the virus. Without this sequence, termed the fusion peptide (FP), the virus is far less effective at fusing with the cellular membrane. One of the interesting features of the isolated FP is that it transitions between an α-helical conformation and a β-sheet conformation in lipid bilayer membranes as a function of lipid composition and concentration, and the transition correlates with fusion. To better understand how the conformations of the FP impact lipid bilayer membranes, a variant of the FP that does not strongly promote fusion, termed gp41rk, was studied. Circular dichroism spectroscopy, dynamic light scattering, small-angle neutron scattering (SANS) and neutron spin echo spectroscopy (NSE) were used to relate the conformation of gp41rk to the structure and mechanical properties of lipid bilayer membrane vesicles composed of a 7:3 molar ratio mixture of 1,2-dimyristoyl-sn-glycero-3-phosphocholine and 1,2-dimyristoyl-sn-glycero-3-phospho-(1'-rac-glycerol). At a peptide-to-lipid ratio (P/L) of 1/200, it adopts an α-helical conformation, while gp41rk is a β-sheet at a P/L of 1/50 in the unilamellar vesicles. SANS reveals that the lipid bilayer membrane becomes thicker when gp41rk adopts a β-sheet conformation, which indicates that the high-concentration state of the peptide increases the order of the lipid acyl chains. At the same time, NSE demonstrates that the bilayer becomes more rigid, demonstrating that the β-sheet conformation, which correlates with fusion for the native FP sequence, stiffens the bilayer. The results have implications for the function of the FP.

Keywords: HIV-1 fusion peptide, neutron spin echo spectroscopy, bilayer dynamics, membrane rigidity.

1. Introduction

The glycoprotein gp41 from the envelope of HIV-1 interacts with the target cell membrane to affect fusion and initiate infection [1]. The 23-residue sequence at the N-terminus of gp41, referred to as the fusion peptide (FP), is of particular importance for fusion because it anchors the virus to the membrane of the target cell [1]. Changing the FP sequence (AVGIGALFLGFLGAAGSTMGARS), such as by changing hydrophobic amino acids to polar amino acids, decreases the ability of the virus to fuse with a target cell membrane [2-5]. As a result, the interaction of peptides having the wild-type FP sequence and mutations with lipid bilayer membranes have been studied by a variety of biophysical experimental techniques [6-14]. The wild-type FP causes fusion to take place in a peptide concentration-dependent and lipid composition-dependent manner, which is also true for some point mutations. Similarly, when a point mutation results in a less effective full-length gp41 glycoprotein, the isolated FP is less fusogenic.

Interestingly, the HIV-1 gp41 FP and mutant peptides display a conformation that depends on the lipid composition and the peptide concentration. Neutral phospholipids and lower peptide concentrations tend to result in the peptides being associated with the lipid bilayers as α-helices [6, 8-10]. The β-sheet conformation, which correlates with fusion, is prevalent at higher peptide concentrations, or when the lipid bilayers contain charged lipids [6, 8, 9, 12, 15] or cholesterol [16], or when divalent cations are present [8, 10, 13]. Similar behavior has been observed for the Ebola fusion peptide [17] and the fusion peptide from the PIV5 paramyxovirus [18]. In the case of the HIV-1 FP, the results strongly suggest that the β-sheet conformation is changing the lipid bilayer in a way that promotes fusion.

Previously, a variant of the HIV-1 gp41 FP was developed to investigate how the β-sheet conformation of the peptide impacts the structure of the lipid bilayer [15]. The peptide, named gp41rk and having the sequence RKGIGALFLGFLGAAGSTMKR, maintains 17 amino acids from the wild-type sequence, but replaces the initial two and final four amino acids in the sequence with two charged amino acids at both locations. While it does not induce fusion in lipid bilayer vesicles composed of a 7:3 molar ratio mixture of 1,2-dimyristoyl-*sn*-glycero-3-phosphocholine (DMPC) and 1,2-dimyristoyl-*sn*-glycero-3-phospho-L-serine (DMPS) at the concentrations studied, it associates with the vesicles as an α-helix at a peptide-to-lipid ratio (P/L) of 1/200 and as a β-sheet at a P/L of 1/50 [15]. Further, small-angle neutron scattering (SANS) revealed that gp41rk caused localized thickening of the bilayer that indicates a peptide-induced change in the local curvature of the bilayer [15].

The previously-observed localized thickening suggested that at least some of the lipid acyl chains became more ordered [15], which may also result the lipid bilayer becoming more rigid. To investigate this possibility, neutron spin echo spectroscopy (NSE) was applied to gp41rk in vesicles composed of a 7:3 molar ratio mixture of DMPC and 1,2-dimyristoyl-*sn*-glycero-3-phospho-(1'-rac-glycerol) (DMPG). The peptide undergoes a concentration-dependent conformational change from an α-helix to a β-sheet in the 7:3 DMPC:DMPG vesicles and SANS reveals a correlated increase in the average total thickness of the bilayer, consistent with previous results [15]. The SANS results indicate that the vesicles in the presence of both the α-helical and β-sheet forms of gp41rk have a thicker core than the peptide-free bilayer possesses, suggesting an increase in lipid chain order. The changes in peptide conformation and in the membrane structure are accompanied by a change in the dynamics of the vesicles, which was measured by NSE. While the α-helical conformation does not change the vesicle dynamics, the β-sheet conformation

resulted in slower vesicle dynamics, indicative a more rigid bilayer. The higher peptide concentration must possess some responsibility for the increased rigidity. However, as the SANS results suggest that both peptides increase the ordering of the lipid chains, the specific interaction of the β-sheet conformation of gp41rk with the membrane must play a large role in the observed change in bilayer rigidity.

2. Materials and Methods

Materials. The amidated form of the gp41rk peptide, having the sequence RKGIGALFLGFLGAAGSTMKR, was synthesized by GenScript (Piscataway, NJ, USA). The peptide, which was used without further purification, was supplied at 91.2% purity. Stock solutions of gp41rk were prepared in 2,2,2-trifluoroethanol (TFE) for preparing the lipid vesicle solutions with peptide. 1,2-dimyristoyl-*sn*-glycero-3-phosphocholine (DMPC; product 850345) and 1,2-dimyristoyl-*sn*-glycero-3-phospho-(1'-rac-glycerol) (DMPG; product 840445) were purchased from Avanti Polar Lipids, Inc. (Alabaster, AL). Chloroform from Amresco, LLC (Solon, OH) was purchased from VWR International, LLC (Radnor, PA), TFE was purchased from Fisher Scientific USA (Pittsburg, PA, USA), and D_2O (99.8% D) was obtained from Cambridge Isotope Laboratories, Inc. (Tewksbury, MA, USA). These chemicals were used without further purification.

Vesicle Solution Preparation. Preparation of vesicles followed the method used in previous studies [15, 19-22]. Samples for the experiments were prepared to have a consistent lipid concentration (20 mg/mL for NSE, SANS and DLS, and 14.4 mg/mL for CD) regardless of the peptide concentration. Peptide was added to provide peptide-to-lipid ratios (P/L) of 1/50 and 1/200

for the SANS, NSE and DLS and 1/50, 1/75, 1/100, 1/150 and 1/200 for the CD measurements. A peptide-free vesicle sample was also prepared for all experiments. Appropriate amounts of lipid and peptide stock solutions were added to provide the desired molar ratios. An additional ~1 mL of 3:1 chloroform:TFE was added to the samples to ensure mixing of lipid and peptide. Then, the organic solvent was blown off under a stream of dry N_2. Samples were freeze dried overnight to remove any residual organic solvent. D_2O was added to the samples to achieve the desired lipid concentrations. The samples were subjected to three freeze-thaw cycles between -80 °C and 40 °C, with extensive vortex mixing before freezing. After the final thawing, the unilamellar vesicles were extruded at least 21 times with an Avanti Polar Lipids, Inc. (Alabaster, AL) mini-extruder fit with a polycarbonate membrane with 100 nm diameter pores. Samples that were not used immediately were stored for up to 24 hours in an incubator set at 12 °C to avoid freezing the samples (D_2O freezes at ~4 °C). In the case of the NSE measurements, which were much longer than the other experiments, the samples were prepared the day before the sample was scheduled to be measured to ensure consistency.

Solution Circular Dichroism. All spectra were collected using a Jasco J-810 CD spectropolarimeter (Tokyo, Japan) having a Jasco PFD-425S Pelletier temperature controller set at 37 °C. Vesicle solutions were measured in 0.1 mm path length, detachable window quartz sample cells from Hellma (Müllheim, Germany), which reduces the artefacts resulting from light scattering by the vesicles. CD data were collected from 180 nm to 260 nm using a step size of 0.5 nm and 10 spectra were averaged. Data collected with gp41rk were corrected for the background signal of the peptide-free vesicles.

Dynamic Light Scattering. Dynamic light scattering (DLS) were performed with a Wyatt Technology Corporation (Santa Barbara, CA) DynaPro Nanostar instrument at a temperature of 37 °C. A series of measurements were made for each sample on the day of extrusion, the following day, and 12 days after extrusion, which is far longer the period of time required for measurement of a single sample by NSE (~3 days). All measurements were made at the same concentration as the SANS and NSE (20 mg/mL), which can result in an apparent decrease in the measured hydrodynamic radius, R_H. The instrument performed 10 acquisitions per sample. The values reported are the averages and standard deviations of the 10 acquisitions.

Small-Angle Neutron Scattering Measurements. The EQ-SANS instrument of the Spallation Neutron Source at Oak Ridge National Laboratory [23] was used for the small-angle neutron scattering (SANS) measurements. Vesicle solutions and the associated D_2O background were measured. All measurements utilized the same instrument configuration: a 4m sample-to-detector distance with the choppers operating at 30 Hz, which provides two bands of neutrons (2.5 Å to 6.1 Å and 9.4 Å to 13.1 Å). The configuration provides $q = 4\pi\sin(\theta)/\lambda$, where 2θ is the scattering angle and λ is the neutron wavelength, from ~0.004 $Å^{-1}$ to ~0.45 $Å^{-1}$. The sample temperature was maintained at 37 °C. All data reduction and merging into $I(q)$ vs. q employed the standard procedures implemented in the MANTID software package [24]. Scaling the data into absolute units of 1/cm employed a calibrated porous silica standard [25].

SANS Data Analysis. The SANS data analysis approach built upon the polydisperse core, multishell spherical modeling method and software employed previously [15, 19-22], but used a different model for the bilayer profile, which is described below. Data were modeled over a q-

range of 0.01 $Å^{-1}$ to 0.35 $Å^{-1}$, which excludes portions of the data (below 0.01 $Å^{-1}$ and above 0.35 $Å^{-1}$) that generally display the effects of inelastic neutron scattering processes in the sample that are observed on time-of-flight SANS instruments [26]. The resolution function of the instrument, which was provided with the reduced data, was convoluted with the model profiles prior to comparison against the SANS data. The quality of the fit of the model to the data was evaluated with the fitting parameter employed previously [27, 28].

The bilayer profile model employed in all cases was a three layer model that correspond to an inner head group (HG) region, a hydrocarbon chain (HC) region, and an outer HG region. This simpler model was employed in the present study because no deuterium-labeled lipids were used for the NSE study, unlike the previous study of gp41rk [15]. The variables for the fitting were the thicknesses and scattering length densities of the three layers. The inner core radius and its polydispersity were also free parameters, although the latter two were generally fixed during the later refinement runs performed (described below). The inner core radius of the vesicles was assumed to have a Gaussian polydispersity. The profile scale factor and a constant baseline were also free parameters during the data fitting.

The data fitting software used a modified simulated annealing method that began with 50 temperature steps that tested 2500 models, which were subsequently followed by another 50 temperature steps that tested 200 models per temperature. The convergence and reproducibility of the fitting were investigated by performing 100 independent fitting runs, the results of which were output by the program for further analysis. Initial runs of the modeling employed broad constraints on all of the free parameters. The results of the initial runs were used for additional refinement runs based around parameter values that provided the best fits to the data from the previous run. The refinement process was performed four times. The averages and standard deviations from the

resulting set of parameters from the converged models from the set of fifth refinement runs, as estimated by the quality of the fit, were calculated and are the values reported herein.

Neutron Spin Echo Spectroscopy Measurements. NSE measurements were performed at the SNS-NSE neutron spin echo spectrometer at the Oak Ridge National Laboratory [29]. The samples were loaded into 4 cm by 4 cm quartz Hellma cells having a 4 mm path length. The temperature was set to 37° C or 18° C, which was only measured for P/L = 1/200, and controlled with a precision of ±0.5° C using a ThermoJet ES system (SP Scientific, Warminster, PA). Two incident neutron beam wavelength bands were used: 5-8 Å and 8-11 Å, which covered Fourier times from approximately 30 ps to 100 ns over a q-range of approximately 0.06 $Å^{-1}$ to 0.15 $Å^{-1}$. A total of 8 q-values were obtained, except for the one sample measured at 18° C. The instrument resolution was measured with graphite foil. D_2O was measured for background subtraction. Data reduction to produce the dynamic structure factor $S(q,\tau)$ was performed with DrSPINE [30].

NSE Data Analysis. The intermediate structure function, $S(q,\tau)/S(q,0)$ was fit according to the stretched exponential form of Zilman and Granek [31] for lipid bilayer vesicles. The function, which is shown in Equation 1, is valid when $qR >> 1$, where R is the radius of the vesicles, which is satisfied here.

$$\frac{S(q,\tau)}{S(q,0)} = e^{-[\Gamma(q)\tau]^{2/3}} \tag{1}$$

In Equation 1, $\Gamma(q)$ is the q-dependent relaxation rate. Rather than using the original theory of Zilman and Granek for $\Gamma(q)$ [31], the form of $\Gamma(q)$ is taken from the later work of Watson and Brown [32], which is shown in Equation 2. Equation 2 accounts for friction between the leaflets

of the bilayer and has been used by other researchers to describe dynamics of lipid bilayer vesicles [33, 34].

$$\Gamma(q) = 0.025\gamma \left(\frac{k_B T}{\tilde{\kappa}}\right)^{\frac{1}{2}} \frac{k_B T}{\eta_{D_2O}} q^3 \tag{2}$$

The viscosity of D_2O, η_{D_2O}, is 0.837 cP at 37 °C and 1.322 cP at 18 °C [35], and k_B is the Boltzmann constant. Here, the value of γ, which was originally described as a weakly increasing function of the temperature, T, [31] is assumed to be unity in the present work, as others have done [33, 34, 36]. The effective bending modulus, $\tilde{\kappa}$, is related to the bending modulus, κ, and the compressibility modulus, k_m, through Equation 3 [32].

$$\tilde{\kappa} = \kappa + 2d^2 k_m \tag{3}$$

The parameter d is the height of the neutral surface of the bilayer from its midplane. It is generally considered to have a value between one half and the full monolayer thickness, but the actual value is not known [32]. In the case of lipid bilayers, the values of κ and k_m, are also related through $\kappa = \beta {d_{hc}}^2 k_m$ [37], where d_{hc} is the thickness of the hydrocarbon region of the bilayer. The factor β is a measure of the degree to which distortions in one leaflet cause distortions in the other leaflet, i.e. the degree of coupling. Lee and coworkers derived relationships between $\tilde{\kappa}$, κ, and k_m [33], which are shown in Equations 4 and 5.

$$\kappa = \frac{\tilde{\kappa}}{[1+((2d/d_{hc})^2/4\beta)]} \tag{4}$$

$$k_m = \frac{\tilde{\kappa}}{[d_{hc}^2(\beta+(2d/d_{hc})^2)/4]} \tag{5}$$

3. Results

The solution CD spectra of gp41rk associated with the 7:3 DMPC:DMPG vesicles are shown in Figure 1. The noise in the spectra are the result of the relatively low peptide

concentrations measured and the 0.1 mm path length cell used to minimize artifacts due to light scattering by the vesicles. None of the data are consistent with a random coil conformation [38], which the peptide adopts when it is in aqueous solution without vesicles (see Figure 1 of reference [15]). The series of concentrations measured, which ranges from P/L = 1/200 to P/L = 1/50, show a clear transition that takes place between P/L = 1/150 and P/L =1/100. For P/L = 1/150 and below, the CD spectrum indicates that the peptide is in a predominantly α-helical conformation, based on the two negative bands near 208 nm and 222 nm [38]. When P/L = 1/100 and higher, the peptide transitions to an antiparallel β-sheet conformation [38]. The present results are consistent with a previous study of gp41rk associated with 7:3 DMPC:DMPS vesicles at both P/L = 1/200 and 1/50 [15], and indicate that the peptide is bound to the vesicles in both conformational states. The CD data provide very little indication of gp41rk adopting a conformation state that is a clearly a mixture of the low and high concentration states, such as has been observed for the peptide alamethicin when studied in oriented multilamellar stacks of lipid bilayers [39]. A concentration-dependent conformational transition was also observed for the wild-type gp41 FP and other variants [6, 8, 40].

DLS was performed to characterize the stability of NSE samples, which are produced at relatively high concentrations compared to previous study of gp41rk [15], over the long measurement times required. The results are presented in Table 1 and indicate that the vesicles are not growing over time, which would be indicative of fusion over periods of time greater than the 3-day duration of a single NSE measurement. It is possible that the decrease in size of the peptide-free vesicles between Day 1 and Day 2 is due to the relatively high concentration used for the NSE measurements. As is noted in Table 1, the NSE experiments began on Day 2 and the samples may have required time to equilibrate. The difference in R_H was not observed in the

samples with gp41rk. In light of the changes in bilayer structure observed by SANS (described below), it is possible that the peptide allowed the vesicles to equilibrate faster. The difference in the R_H as a function of peptide concentration is significant. A decrease in R_H with increasing vesicle concentration was observed previously by this group [22] and can be attributed to particle-particle interactions. Increasing amounts of peptide reduce the net charge of the vesicles, which results in less electrostatic vesicle-vesicle repulsion and can be the cause of the change in R_H with peptide concentration. The previous study was of melittin and used a maximum P/L of 1/200, so the peptide concentration may have been too low to impact the observed R_H by changing the vesicle-vesicle interactions [22].

Peptide-induced changes in bilayer structure were studied by SANS for P/L = 1/200 and 1/50. The SANS data are presented in Figure 2, along with the fit curves resulting from the modeling that is described in the Materials and Methods. The data are also presented in Figure 2 over an abbreviated q-range and without any offset applied to highlight the differences in the data in the q-range that arises from the bilayer structure. The SANS data indicate that the bilayer structure changes when gp41rk is present in the system, but the differences between the P/L = 1/200 and P/L = 1/50 data sets are considerably more subtle than how either data set differs from the data collected when no gp41rk was present. The results of the SANS data modeling are presented in Table 2. While not the focus of this study, the data collected at 18 °C for all samples and the associated modeling results are also presented in Figure 2 and Table 2, respectively, to provide points of reference for the interpretation of the SANS and NSE data collected at 37 °C. The single profile collected in the present study results in data that is less information-rich than SANS data obtained in previous studies that employed contrast variation methods with selective deuterium labeling [15, 19-21]. As a result, the layer thicknesses and scattering length densities

of the membrane are less robust due to the lack of distinctive features in the data for $q > 0.10$ Å^{-1}, but the overall thickness is a robust parameter. At P/L = 1/200, the total thickness of the bilayer is unchanged, but the core of the bilayer becomes thicker while the inner and outer polar regions become thinner. The scattering length densities of the inner polar region and core increase significantly, suggesting the possibility that the α-helical state of gp41rk spans the bilayer. As can be seen in Table 2, when P/L = 1/50, the bilayer measured at 37 °C is thicker than it is when gp41rk is not present or when P/L = 1/200. The total thickness is more consistent with the thicknesses determine for the samples measured at 18 °C. While the core remains thicker than that of the peptide-free bilayer, the majority of the thickness increase is in the outer polar region, which suggests that the β-sheet conformation of gp41rk associates with the surface of the vesicle. The modeling results also show a decrease in the scattering length density of the core when gp41rk is present at P/L = 1/50 relative to the value at P/L = 1/200, supporting gp41rk being associated, at least in part, with the vesicle surface.

The $S(q,\tau)/S(q,0)$ vs. τ that were measured by NSE are presented in Figure 3, and the resulting Γ/q^3 vs. q are shown in Figure 4. The average values of Γ/q^3 and the resulting values of $\tilde{\kappa}$ obtained using Equation 2 are presented in Table 3. As can be seen in Figure 3, the data collected for peptide free 7:3 DMPC:DMPG vesicles and that collected when gp41rk was present at P/L = 1/200 are very similar. Γ/q^3 and $\tilde{\kappa}$ for these samples are the same to within the experimental uncertainty. As expected, when the temperature of the P/L = 1/200 sample was lowered below the gel phase transition temperature of the lipid, the NSE data and resulting values of Γ/q^3 and $\tilde{\kappa}$ reflect a much more rigid peptide-containing vesicle. At P/L = 1/50, $S(q,\tau)/S(q,0)$ decays slower than the data for the other two peptide concentrations studied, but the difference is not nearly as dramatic as it is for the gel phase sample at P/L = 1/200. The results demonstrate that gp41rk at

this concentration, which results in the β-sheet conformation of the peptide, caused the vesicles to be appreciably more rigid, as measured by $\tilde{\kappa}$ that is presented in Table 3. At P/L = 1/50, $\tilde{\kappa}$ is 67% greater than without gp41rk or at P/L =1 /200.

4. Discussion

The present CD and SANS results are consistent with the results of the previous study of gp41rk in 7:3 DMPC:DMPS vesicles [15], even though the head groups of DMPS and DMPG are structurally dissimilar. Similar lipid-independent behavior was previously observed for the wild-type FP in 4:1 molar ratio mixtures of 1-palmitoyl-2-oleoyl-*sn*-glycero-3-phosphocholine (POPC) with either 1-palmitoyl-2-oleoyl-*sn*-glycero-3-phospho-L-serine (POPS) or 1-palmitoyl-2-oleoyl-*sn*-glycero-3-phospho-(1'-rac-glycerol) (POPG), but only when 30 mol% cholesterol was added [40]. The results indicate that the presence of charged lipids, rather than specific lipid chemistry, drives the transition of gp41rk between conformations. The peptide penetratin [41], a 16 amino acid long peptide that is part of the third helix of the Drosophila antennapedia homeodomain that has the sequence RQIKIWFQNRRMKWKK, also transitions between an α-helix and a β-sheet when associated with lipid bilayers [42-45]. The transition is concentration-dependent and the critical concentration depends on the lipid composition [42-44]. In vesicle solutions, charged lipids are essential for enabling the conformational transition [42, 43]. The critical concentration also depends on the acyl chain composition, as was observed in hydrated lipid bilayer films [44]. A lower critical concentration was observed for lipids having fully saturated chains compared to when the bilayer contained unsaturated lipids [44]. Unlike gp41rk, which causes the bilayer to become thicker when in the β-sheet conformation, penetratin thins the bilayer when it is in the α-helical state and the bilayer thickness returns to its normal thickness when the peptide is in the β-

sheet conformation at high concentration [44]. Even though penetratin is shorter, carries a higher positive charge and is less hydrophobic than gp14rk, their interaction with membranes shares common features. It is rather surprising because gp41rk derives from a fusion peptide from a viral coat protein [1] and penetratin is a cell-penetrating peptide derived from a DNA-binding domain of a transcription factor [41].

Determining the values of κ and k_m using Equation 4 and 5 [33] can help understand how the bilayer is changing in response to the conformational change of gp41rk. These relations rely on two parameters that cannot be readily measured, namely β, the measure of interleaflet coupling, and d, the height of the neutral surface of the bilayer. As a result, we rely of values employed by others. Values for β range from 1/12 for fully-coupled bilayer leaflets and 1/48 when the leaflets of the bilayer are not coupled [37]. Experiments have determined that $\beta = 1/24$ for both saturated and unsaturated lipid bilayers that do not have incorporated proteins, which is in agreement with the value predicted using a polymer brush model [46], and was assumed in the interpretation of NSE data from lipid bilayer vesicles containing the peptide melittin [33]. For the interpretation of the NSE data presented herein, we assume that $\beta = 1/24$. The value of $2d/d_{hc}$ must also be estimated because d is not exactly known [32] and is likely impacted by the bound gp41rk. Based on measurements of pure DOPC, Lee and coworkers estimated $2d/d_{hc} = 1.21$, where d_{hc} is the thickness of the hydrocarbon region of the bilayer [33] . This value was used by Woodka and coworkers to interpret NSE data from DMPC [34]. However, Nagao and coworkers employed $2d/d_{hc} = 1.0$ in a later study of saturated phosphatidylcholine lipids, including DMPC [36]. Here, values of $2d/d_{hc}$ = from 1.00 to 1.21 were considered for use in the interpretation of the NSE results. Under the aforementioned set of assumptions, the ranges of values of κ and k_m are presented in

Table 3. The change in κ with peptide concentration mirrors the change in $\tilde{\kappa}$. In contrast, the k_m is less impacted by the highest concentration of gp41rk studied.

The peptide-free 7:3 DMPC:DMPG lipid bilayer vesicles are less rigid than vesicles composed of DMPC that were studied by NSE [33, 34], which is consistent with a recent atomic force microscopy study of the effects of charged lipids on the mechanical properties of vesicles [47]. The fact that both the vesicle and the bilayer become more rigid in the presence of gp41rk is an interesting result. In contrast, similar concentrations of melittin resulted in 1,2-dioleoyl-sn-glycero-3-phosphocholine (DOPC) bilayers that were less rigid than peptide-free DOPC [33]. Melittin is α-helical when associated with lipid bilayers, but does undergo a transition between a surface-adsorbed state that results in increased acyl chain disorder, which is found at low P/L, and a pore-forming, membrane-spanning state that is present at higher peptide concentrations [48, 49]. Lee and coworkers attributed the decrease in vesicle and bilayer rigidity to the increased acyl chain disorder at low concentration, which persisted due to the relatively low concentration of pores that coexisted with surface-adsorbed peptides when melittin was present at P/L = 1/50 [33]. The peptide alamethicin also softened lipid bilayer membranes composed of a single lipid, specifically DOPC [50], 1,2-dilauroyl-sn-glycero-3-phosphocholine (DLPC) [51] and 1,2-diphytanoyl-sn-glycero-3-phosphocholine (DPhPC) [51]. Alamethicin also creates more disordered acyl chains, particularly at low concentration when it is not forming transmembrane pores [52]. The present results demonstrate that the interaction of gp41rk differs from these archetypal α-helical membrane-active peptides.

The present work and the previous investigation of gp41rk in 7:3 DMPC:DMPS bilayers where deuterium-labeled DMPC was used [15] support the idea that gp41rk interacts with the lipid acyl chains and makes them more, rather than less, ordered. In both cases, the β-sheet

conformation found at high concentration created the largest impact on the structure. The previous investigation using chain perdeuterated lipids revealed that regions of the lipid bilayer became thicker when gp41rk was present at P/L = 1/50, suggesting localized ordering of the lipid acyl chains [15]. Although the present work did not use deuterium labeling, the SANS results reveal that the thicknesses of both the core and polar regions also increased, which supports an increase in average lipid acyl chain order that would produce a correspondingly more rigid vesicle. These results seem counter to the model for the interaction of the gp41 FP presented by Qiang and coworkers [16], specifically that shown in Figure 3 of the paper, which has the peptide adsorbed into the HG region of the bilayer and penetrating to various depths because the chains should become more disordered to fill in the space under the peptides, resulting in a thinner bilayer. They found that sequence-dependent peptide-driven fusion correlates with the depth of penetration into the membrane [16]. While the mode of interaction seems similar to alamethicin or melittin [49], it remains possible that such an interaction causes the acyl chains to order, rather than disorder.

Increasing, rather than decreasing the rigidity of the bilayer appears counterintuitive to facilitating the morphological changes needed for fusing a virus and cell or two vesicles. However, increasing the rigidity of the lipid bilayer membrane increases the free energy cost of additional distortions to the membrane, such as take place as a result of additional interactions forming as the vesicle and cell form additional contacts or as vesicles collide. Fusion peptides exert their effects locally. As was noted in the previous study of gp41rk [15], while a minority fraction of the lipid bilayer in the vesicles became thicker when P/L = 1/50, the remainder of the lipid bilayer actually became thinner, indicating an increase in the disorder of the lipid acyl chains that results in the rest of the vesicle becoming more flexible and therefore easier to distort in a manner that allows fusion to take place.

5. Conclusions

NSE revealed that the β-sheet conformation of gp41rk results in a more rigid lipid bilayer, This result is in stark contrast to behavior observed for alamethicin and melittin, which soften lipid bilayer membranes by increasing the disorder of the acyl chains [33, 50, 51]. The cause of the stiffening is more ordered lipid acyl chains that resulted in the increased lipid bilayer thickness that was revealed by SANS and was observed previously [15]. While gp41rk is not fusogenic at the concentrations studied, the results suggest a mechanism through which the helix-to-sheet transition of gp41 could facilitate fusion.

Acknowledgements

The authors would like to thank M. Cochran for assistance during the NSE experiments, C. Gao during the EQ-SANS experiments and H. M. O'Neill for access to the CD instrument. This research used resources at the Spallation Neutron Source, A DOE Office of Science User Facility operated by the Oak Ridge National Laboratory. Neutron beam time for this research has been allocated by the Jülich Center for Neutron Science, JCNS1, Jülich Forschungszentrum GmbH, Germany, outstation to the Spallation Neutron Source (SNS), Oak Ridge, TN.

References

[1] E.O. Freed, M.A. Martin, The role of human-immunodeficiency-virus type-1 envelope glycoproteins in virus-infection, J. Biol. Chem., 270 (1995) 23883-23886.

[2] J.M. Felser, T. Klimkait, J. Silver, A syncytia assay for human immunodeficiency virus type-i (hiv-i) envelope protein and its use in studying hiv-i mutations, Virology, 170 (1989) 566-570.

[3] E.O. Freed, D.J. Myers, R. Risser, Characterization of the fusion domain of the human-immunodeficiency-virus type-1 envelope glycoprotein gp41, Proc. Natl. Acad. Sci. U. S. A., 87 (1990) 4650-4654.

[4] L. Bergeron, N. Sullivan, J. Sodroski, Target cell-specific determinants of membrane-fusion within the human-immunodeficiency-virus type-1 gp120 3rd-variable region and gp41 amino terminus, J. Virol., 66 (1992) 2389-2397.

[5] E.O. Freed, E.L. Delwart, G.L. Buchschacher, A.T. Panganiban, A mutation in the human-immunodeficiency-virus type-1 transmembrane glycoprotein-gp41 dominantly interferes with fusion and infectivity, Proc. Natl. Acad. Sci. U. S. A., 89 (1992) 70-74.

[6] M. Rafalski, J.D. Lear, W.F. Degrado, Phospholipid interactions of synthetic peptides representing the n-terminus of hiv gp41, Biochemistry, 29 (1990) 7917-7922.

[7] V.A. Slepushkin, G.B. Melikyan, M.S. Sidorova, V.M. Chumakov, S.M. Andreev, R.A. Manulyan, E.V. Karamov, Interaction of human-immunodeficiency-virus (hiv-1) fusion peptides with artificial lipid-membranes, Biochem. Biophys. Res. Commun., 172 (1990) 952-957.

[8] J.L. Nieva, S. Nir, A. Muga, F.M. Goni, J. Wilschut, Interaction of the hiv-1 fusion peptide with phospholipid-vesicles - different structural requirements for fusion and leakage, Biochemistry, 33 (1994) 3201-3209.

[9] I. Martin, H. Schaal, A. Scheid, J.M. Ruysschaert, Lipid membrane fusion induced by the human immunodeficiency virus type 1 gp41 n-terminal extremity is determined by its orientation in the lipid bilayer, J. Virol., 70 (1996) 298-304.

[10] F.B. Pereira, F.M. Goni, A. Muga, J.L. Nieva, Permeabilization and fusion of uncharged lipid vesicles induced by the hiv-1 fusion peptide adopting an extended conformation: Dose and sequence effects, Biophys. J., 73 (1997) 1977-1986.

[11] C. Curtain, F. Separovic, K. Nielsen, D. Craik, Y. Zhong, A. Kirkpatrick, The interactions of the n-terminal fusogenic peptide of hiv-1 gp41 with neutral phospholipids, Eur. Biophys. J. Biophys. Lett., 28 (1999) 427-436.

[12] P.W. Mobley, A.J. Waring, M.A. Sherman, L.M. Gordon, Membrane interactions of the synthetic n-terminal peptide of hiv-1 gp41 and its structural analogs, Biochim. Biophys. Acta-Biomembr., 1418 (1999) 1-18.

[13] A. Saez-Cirion, J.L. Nieva, Conformational transitions of membrane-bound hiv-1 fusion peptide, Biochim. Biophys. Acta-Biomembr., 1564 (2002) 57-65.

[14] S. Castano, B. Desbat, Structure and orientation study of fusion peptide fp23 of gp41 from hiv-1 alone or inserted into various lipid membrane models (mono-, bi- and multibi-layers) by ft-ir spectroscopies and brewster angle microscopy, Biochim. Biophys. Acta-Biomembr., 1715 (2005) 81-95.

[15] W.T. Heller, D.K. Rai, Changes in lipid bilayer structure caused by the helix-to-sheet transition of an hiv-1 gp41 fusion peptide derivative, Chem. Phys. Lipids, 203 (2017) 46-53.

[16] W. Qiang, Y. Sun, D.P. Weliky, A strong correlation between fusogenicity and membrane insertion depth of the hiv fusion peptide, Proc. Natl. Acad. Sci. U. S. A., 106 (2009) 15314-15319.

[17] A. Agopian, S. Castano, Structure and orientation study of ebola fusion peptide inserted in lipid membrane models, Biochim. Biophys. Acta-Biomembr., 1838 (2014) 117-126.

[18] H.W. Yao, M. Hong, Membrane-dependent conformation, dynamics, and lipid interactions of the fusion peptide of the paramyxovirus piv5 from solid-state nmr, J. Mol. Biol., 425 (2013) 563-576.

[19] S. Qian, W.T. Heller, Peptide-induced asymmetric distribution of charged lipids in a vesicle bilayer revealed by small-angle neutron scattering, J. Phys. Chem. B, 115 (2011) 9831-9837.

[20] S. Qian, D. Rai, W.T. Heller, Alamethicin disrupts the cholesterol distribution in dimyristoyl phosphatidylcholine-cholesterol lipid bilayers, J. Phys. Chem. B, 118 (2014) 11200-11208.

[21] S. Qian, W.T. Heller, Melittin-induced cholesterol reorganization in lipid bilayer membranes, Biochim. Biophys. Acta-Biomembr., 1848 (2015) 2253-2260.

[22] D.K. Rai, S. Qian, W.T. Heller, The interaction of melittin with dimyristoyl phosphatidylcholine-dimyristoyl phosphatidylserine lipid bilayer membranes, Biochimica et Biophysica Acta (BBA) - Biomembranes, 1858 (2016) 2788-2794.

[23] J.K. Zhao, C.Y. Gao, D. Liu, The extended q-range small-angle neutron scattering diffractometer at the sns, J. Appl. Crystallogr., 43 (2010) 1068-1077.

[24] O. Arnold, J.C. Bilheux, J.M. Borreguero, A. Buts, S.I. Campbell, L. Chapon, M. Doucet, N. Draper, R.F. Leal, M.A. Gigg, V.E. Lynch, A. Markyardsen, D.J. Mikkelson, R.L. Mikkelson, R. Miller, K. Palmen, P. Parker, G. Passos, T.G. Perring, P.F. Peterson, S. Ren, M.A. Reuter, A.T. Savici, J.W. Taylor, R.J. Taylor, R. Tolchenoy, W. Zhou, J. Zikoysky, Mantid-data analysis and visualization package for neutron scattering and mu sr experiments, Nucl. Instrum. Methods Phys. Res. Sect. A-Accel. Spectrom. Dect. Assoc. Equip., 764 (2014) 156-166.

[25] G.D. Wignall, F.S. Bates, Absolute calibration of small-angle neutron-scattering data, J. Appl. Crystallogr., 20 (1987) 28-40.

[26] C. Do, W.T. Heller, C. Stanley, F.X. Gallmeier, M. Doucet, G.S. Smith, Understanding inelastically scattered neutrons from water on a time-of-flight small-angle neutron scattering (sans) instrument, Nucl. Instrum. Methods Phys. Res. Sect. A-Accel. Spectrom. Dect. Assoc. Equip., 737 (2014) 42-46.

[27] W.T. Heller, Ellstat: Shape modeling for solution small-angle scattering of proteins and protein complexes with automated statistical characterization, J. Appl. Crystallogr., 39 (2006) 671-675.

[28] E. Tjioe, W.T. Heller, Ornl_sas: Software for calculation of small-angle scattering intensities of proteins and protein complexes, J. Appl. Crystallogr., 40 (2007) 782-785.

[29] M. Ohl, M. Monkenbusch, N. Arend, T. Kozielewski, G. Vehres, C. Tiemann, M. Butzek, H. Soltner, U. Giesen, R. Achten, H. Stelzer, B. Lindenau, A. Budwig, H. Kleines, M. Drochner, P. Kaemmerling, M. Wagener, R. Moller, E.B. Iverson, M. Sharp, D. Richter, The spin-echo spectrometer at the spallation neutron source (sns), Nucl. Instrum. Methods Phys. Res. Sect. A-Accel. Spectrom. Dect. Assoc. Equip., 696 (2012) 85-99.

[30] P.A. Zolnierczuk, O. Holderer, M. Monkenbusch, Drspine: Data reduction for spin echo experiments, AIP Conference Proceedings, 1969 (2018) 050003.

[31] A.G. Zilman, R. Granek, Undulations and dynamic structure factor of membranes, Phys. Rev. Lett., 77 (1996) 4788-4791.

[32] M.C. Watson, F.L.H. Brown, Interpreting membrane scattering experiments at the mesoscale: The contribution of dissipation within the bilayer, Biophys. J., 98 (2010) L9-L11.

[33] J.H. Lee, S.M. Choi, C. Doe, A. Faraone, P.A. Pincus, S.R. Kline, Thermal fluctuation and elasticity of lipid vesicles interacting with pore-forming peptides, Phys. Rev. Lett., 105 (2010).

[34] A.C. Woodka, P.D. Butler, L. Porcar, B. Farago, M. Nagao, Lipid bilayers and membrane dynamics: Insight into thickness fluctuations, Phys. Rev. Lett., 109 (2012).

[35] R.C. Hardy, R.L. Cottington, Viscosity of deuterium oxide and water in the range 5-degrees-c to 125-degrees-c, J. Res. Natl. Bur. Stand., 42 (1949) 573-578.

[36] M. Nagao, E.G. Kelley, R. Ashkar, R. Bradbury, P.D. Butler, Probing elastic and viscous properties of phospholipid bilayers using neutron spin echo spectroscopy, J. Phys. Chem. Lett., 8 (2017) 4679-4684.

[37] M. Bloom, E. Evans, O.G. Mouritsen, Physical-properties of the fluid lipid-bilayer component of cell-membranes - a perspective, Q. Rev. Biophys., 24 (1991) 293-397.

[38] S. Brahms, J. Brahms, Determination of protein secondary structure in solution by vacuum ultraviolet circular-dichroism, J. Mol. Biol., 138 (1980) 149-178.

[39] Y. Wu, H.W. Huang, G.A. Olah, Method of oriented circular-dichroism, Biophys. J., 57 (1990) 797-806.

[40] A.L. Lai, A.E. Moorthy, Y.L. Li, L.K. Tamm, Fusion activity of hiv gp41 fusion domain is related to its secondary structure and depth of membrane insertion in a cholesterol-dependent fashion, J. Mol. Biol., 418 (2012) 3-15.

[41] D. Derossi, A.H. Joliot, G. Chassaing, A. Prochiantz, The 3rd helix of the antennapedia homeodomain translocates through biological-membranes, J. Biol. Chem., 269 (1994) 10444-10450.

[42] M. Magzoub, L.E.G. Eriksson, A. Graslund, Conformational states of the cell-penetrating peptide penetratin when interacting with phospholipid vesicles: Effects of surface charge and peptide concentration, Biochim. Biophys. Acta-Biomembr., 1563 (2002) 53-63.

[43] M. Magzoub, L.E.G. Eriksson, A. Graslund, Comparison of the interaction, positioning, structure induction and membrane perturbation of cell-penetrating peptides and non-translocating variants with phospholipid vesicles, Biophys. Chem., 103 (2003) 271-288.

[44] C.C. Lee, Y. Sun, H.W. Huang, Membrane-mediated peptide conformation change from alpha-monomers to beta-aggregates, Biophys. J., 98 (2010) 2236-2245.

[45] Y. Sun, C.C. Lee, T.H. Chen, H.W. Huang, Kinetic process of beta-amyloid formation via membrane binding, Biophys. J., 99 (2010) 544-552.

[46] W. Rawicz, K.C. Olbrich, T. McIntosh, D. Needham, E. Evans, Effect of chain length and unsaturation on elasticity of lipid bilayers, Biophys. J., 79 (2000) 328-339.

[47] Y. Takechi-Haraya, Y. Goda, K. Sakai-Kato, Atomic force microscopy study on the stiffness of nanosized liposomes containing charged lipids, Langmuir, (2018).

[48] H.W. Huang, F.Y. Chen, M.T. Lee, Molecular mechanism of peptide-induced pores in membranes, Phys. Rev. Lett., 92 (2004).

[49] H.W. Huang, Molecular mechanism of antimicrobial peptides: The origin of cooperativity, Biochim. Biophys. Acta-Biomembr., 1758 (2006) 1292-1302.

[50] G. Pabst, S. Danner, R. Podgornik, J. Katsaras, Entropy-driven softening of fluid lipid bilayers by alamethicin, Langmuir, 23 (2007) 11705-11711.

[51] V. Vitkova, P. Meleard, T. Pott, I. Bivas, Alamethicin influence on the membrane bending elasticity, Eur. Biophys. J. Biophys. Lett., 35 (2006) 281-286.

[52] K. He, S.J. Ludtke, W.T. Heller, H.W. Huang, Mechanism of alamethicin insertion into lipid bilayers, Biophys. J., 71 (1996) 2669-2679.

Table 1. Hydrodynamic radii, R_H, of the vesicles prepared for the NSE experiments determined by dynamic light scattering. Day 1 corresponds to the day of extrusion, while Day 2 corresponds to the start of the NSE experiments.

	7:3 DMPC:DMPG	**7:3 DMPC:DMPG P/L = 1/200**	**7:3 DMPC:DMPG P/L = 1/50**
Day	**R_H (nm)**	**R_H (nm)**	**R_H (nm)**
1	38.7 ± 1.2	30.7 ± 0.7	39.5 ± 1.5
2	31.6 ± 1.2	29.0 ± 0.7	39.6 ± 1.6
12	28.2 ± 0.8	31.2 ± 1.0	42.5 ± 1.3

Table 2. Results of modeling SANS data. The vesicle layer thicknesses (T_{inner}, T_{core} and T_{outer}), as well as the layer scattering length densities (ρ_{inner}, ρ_{core} and ρ_{outer}) are presented and correspond to the polar region of the inner leaflet, the hydrocarbon core and the polar region of the outer leaflet, respectively. In the case of the peptide-free vesicles, the scattering length density of the shell corresponding to the hydrocarbon core of the bilayer (ρ_{core}) was fixed to the value calculated from the chemical composition of the lipid acyl chains.

T = 37 °C			
	7:3 DMPC:DMPG	**7:3 DMPC:DMPG P/L = 1/200**	**7:3 DMPC:DMPG P/L = 1/50**
T_{inner} (Å)	15.7 ± 0.2	12.9 ± 0.2	11.3 ± 0.2
T_{core} (Å)	12.6 ± 0.6	17.1 ± 1.6	15.6 ± 0.8
T_{outer} (Å)	11.5 ± 0.4	10.3 ± 1.3	16.4 ± 0.6
Total Thickness (Å)	**39.7 ± 0.1**	**40.3 ± 0.2**	**43.2 ± 0.2**
ρ_{inner} (fm/Å^2)	0.333 ± 0.003	0.436 ± 0.021	0.457 ± 0.019
ρ_{core} (fm/Å^2)	-0.037 (fixed)	0.142 ± 0.044	0.035 ± 0.054
ρ_{outer} (fm/Å^2)	0.195 ± 0.007	0.231 ± 0.031	0.341 ± 0.027
T = 18 °C			
	7:3 DMPC:DMPG	**7:3 DMPC:DMPG P/L = 1/200**	**7:3 DMPC:DMPG P/L = 1/50**
T_{inner} (Å)	17.5 ± 0.2	13.3 ± 0.7	10.9 ± 0.7
T_{core} (Å)	4.6 ± 0.2	11.8 ± 0.9	15.4 ± 1.2
T_{outer} (Å)	20.4 ± 0.1	17.0 ± 0.4	16.8 ± 0.9
Total Thickness (Å)	**42.8 ± 0.1**	**42.1 ± 0.1**	**43.1 ± 0.1**
ρ_{inner} (fm/Å^2)	0.192 ± 0.004	0.217 ± 0.022	0.208 ± 0.015
ρ_{core} (fm/Å^2)	-0.037 (fixed)	0.188 ± 0.025	0.151 ± 0.051
ρ_{outer} (fm/Å^2)	0.387 ± 0.002	0.415 ± 0.012	0.400 ± 0.025

Table 3. Average values of Γ/q^3 and $\tilde{\kappa}$ derived from the NSE data, as well as the ranges for the values of κ and k_m determined from $\tilde{\kappa}$ as described in the Materials and Methods. When a range is presented, the lower value corresponds to when $2d/d_{hc} = 1.21$, while the upper value corresponds to when $2d/d_{hc} = 1.00$. These bounding values are described in the Discussion.

	Γ/q^3 (Å^3/ns)	$\tilde{\kappa}/k_BT$	κ/k_BT	k_m (N/m)
7:3 DMPC:DMPG, T = 37 °C	10.6 ± 0.4	145.7 ± 11.6	14.9 ± 1.2 to 20.8 ± 1.7	0.22 ± 0.01 to 0.19 ± 0.02
7:3 DMPC:DMPG P/L = 1/200, T = 37 °C	10.3 ± 0.4	154.3 ± 12.7	15.8 ± 1.3 to 22.1 ± 1.8	0.24 ± 0.01 to 0.21 ± 0.02
7:3 DMPC:DMPG P/L = 1/50, T = 37 °C	8.2 ± 0.4	243.5 ± 25.6	24.9 ± 2.6 to 34.8 ± 3.6	0.30 ± 0.02 to 0.28 ± 0.03
7:3 DMPC:DMPG P/L = 1/200, T = 18 °C	1.3 ± 0.3	3420 ± 1760	349.5 ± 179.9 to 488.5 ± 251.5	3.06 ± 1.57 to 4.28 ± 2.20

Figure Captions

Figure 1. CD data collected for 7:3 DMPC:DMPG vesicles with gp41rk at P/L = 1/200 (black), P/L = 1/150 (red), P/L = 1/100 (green), P/L = 1/75 (blue) and P/L = 1/50 (cyan).

Figure 2. SANS data collected at (A) 37 °C and (B) 18 °C for 7:3 DMPC:DMPG with no peptide (black squares) and gp41rk at P/L = 1/200 (red circles) and 1/50 (blue triangles). The black curves are example fits to the data using the 3-shell model. The P/L = 1/200 and 1/50 have been offset vertically in panels A and B for clarity. The region of the data that arises from the bilayer structure is highlighted for (C) 37 °C and (D) 18 °C without the use of offsets. The symbols used correspond to the same samples as they do in panels (A) and (B).

Figure 3. $S(q,\tau)/S(q,0)$ for 7:3 DMPC:DMPG at 37 °C for P/L = 0 (A), 1/200 (B) and 1/50 (C). Data collected at 18 °C for P/L = 1/200 (D) are also presented. In panels A-C, the symbols correspond to q = 0.059 Å^{-1} (black squares), 0.065 Å^{-1} (red circles), 0.072 Å^{-1} (blue up triangles), 0.089 Å^{-1} (green down triangles), 0.098 Å^{-1} (violet diamonds), 0.108 Å^{-1} (gold left triangles), 0.121 Å^{-1} (cyan right triangles) and 0.140 Å^{-1} (brown hexagons). In panel D, the symbols correspond to q = 0.055 Å^{-1} (black squares), 0.063 Å^{-1} (red circles), 0.074 Å^{-1} (blue up triangles), 0.082 Å^{-1} (green down triangles), 0.095 Å^{-1} (violet diamonds) and 0.110 Å^{-1} (gold left triangles).

Figure 4. Γ/q^3 vs. q for 7:3 DMPC:DMPG vesicles at 37 °C (black squares) and with gp41rk at P/L = 1/200 (red circles) and 1/50 (blue up triangles). Results from gp41rk at P/L = 1/200 taken at 18 °C are also presented (green down triangles). The dashed lines are provided as guides for the eye and are located at the average values presented in Table 3.

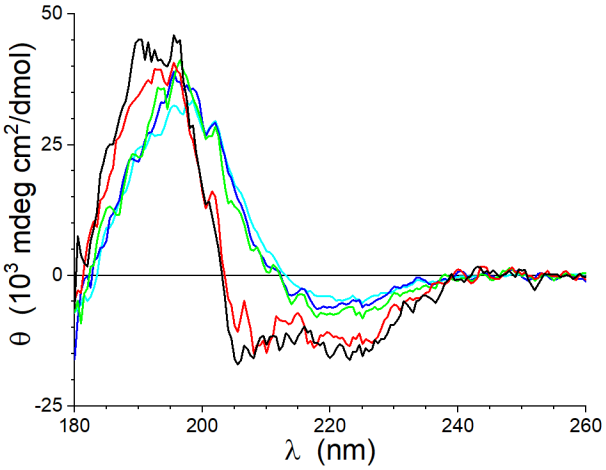

Figure 1

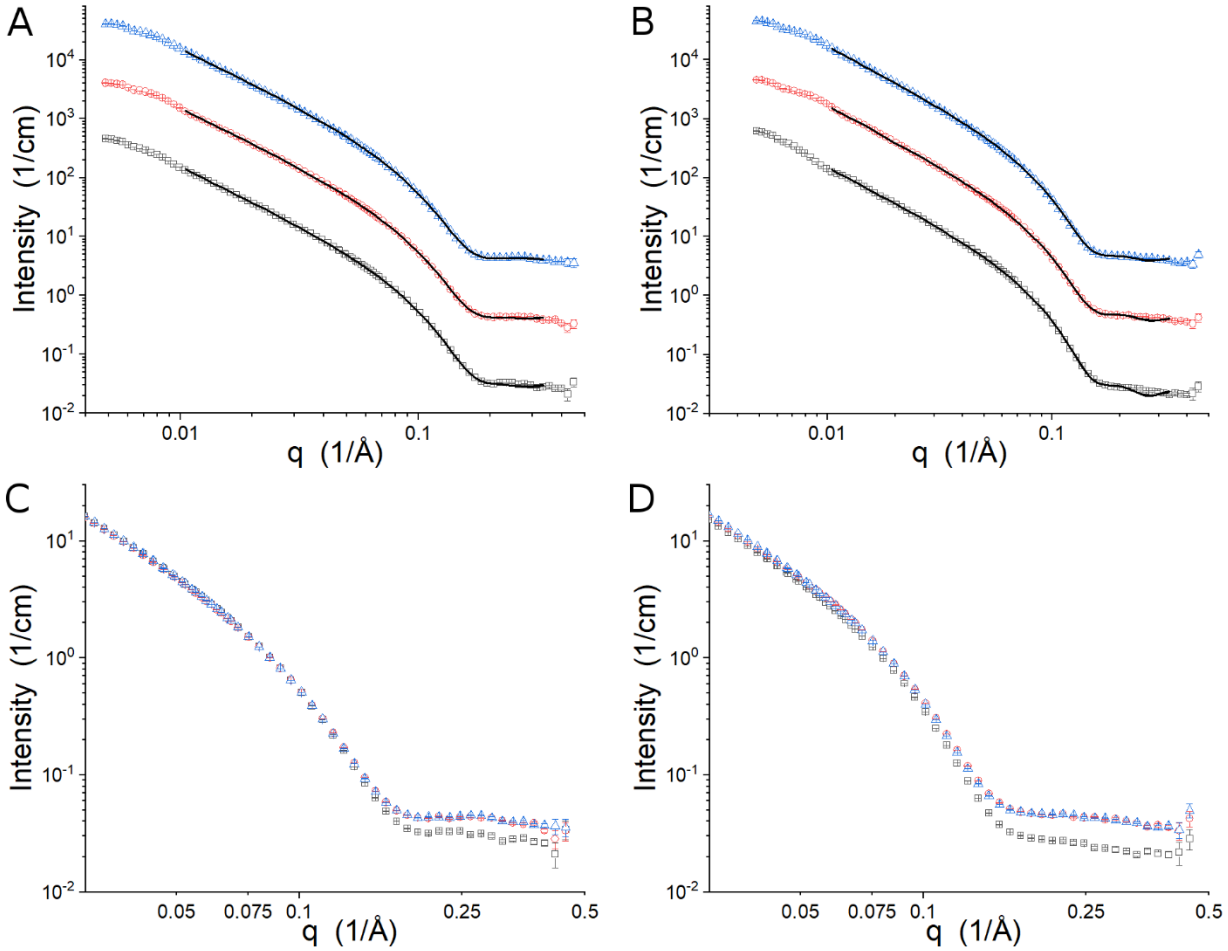

Figure 2

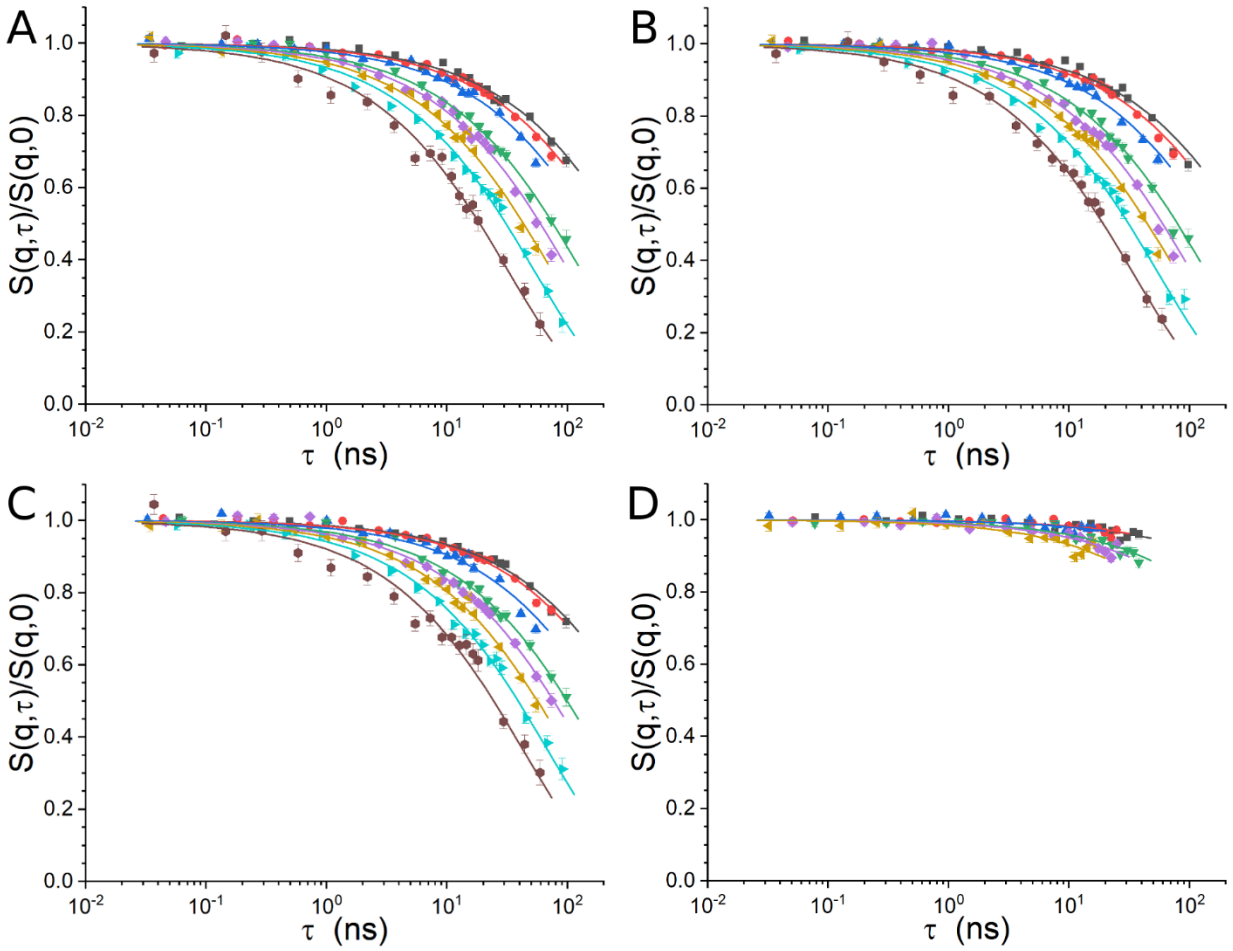

Figure 3

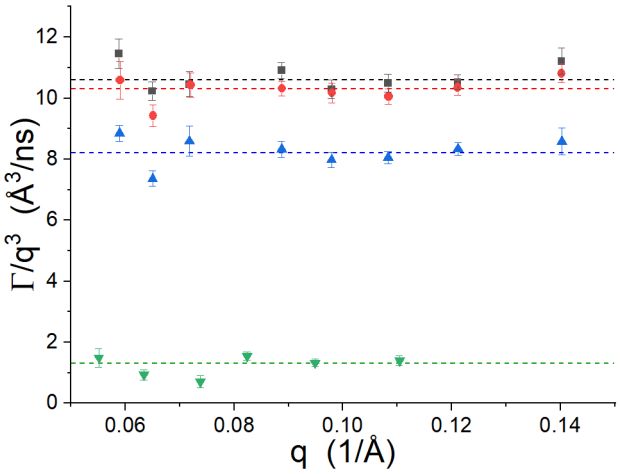

Figure 4

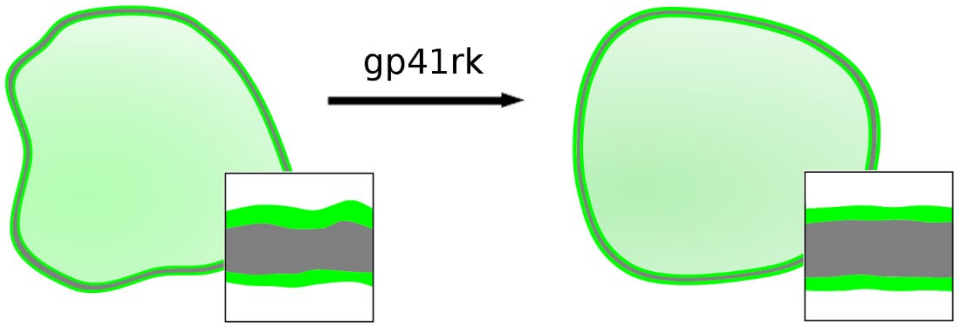

Table of Contents Graphic